Suprem R. Das#, Sajia Sadeque#, Changwook Jeong, Ruiyi Chen, Muhammad A. Alam*, and David B. Janes*

Copercolating Networks: An Approach for Realizing High-Performance Transparent Conductors using Multicomponent Nanostructured Networks

DOI 10.1515/nanoph-2016-0036
Received October 20, 2015; accepted March 21, 2016

Abstract: Although transparent conductive oxides such as indium tin oxide (ITO) are widely employed as transparent conducting electrodes (TCEs) for applications such as touch screens and displays, new nanostructured TCEs are of interest for future applications, including emerging transparent and flexible electronics. A number of two-dimensional networks of nanostructured elements have been reported, including metallic nanowire networks consisting of silver nanowires, metallic carbon nanotubes (mCNTs), copper nanowires or gold nanowires, and metallic mesh structures. In these single-component systems, it has generally been difficult to achieve sheet resistances that are comparable to ITO at a given broadband optical transparency. A relatively new third category of TCEs consisting of networks of 1D-1D and 1D-2D nanocomposites (such as silver nanowires and CNTs, silver nanowires and polycrystalline graphene, silver nanowires and reduced graphene oxide) have demonstrated TCE performance comparable to, or better than, ITO. In such hybrid networks, copercolation between the two components can lead to relatively low sheet resistances at nanowire densities corresponding to high optical transmittance. This review provides an overview of reported hybrid networks, including a comparison of the performance regimes achievable with those of ITO and single-component nanostructured networks. The performance is compared to that expected from bulk thin films and analyzed in terms of the copercolation model. In addition, performance characteristics relevant for flexible and transparent applications are discussed. The new TCEs are promising, but significant work must be done to ensure earth abundance, stability, and reliability so that they can eventually replace traditional ITO-based transparent conductors.

Keywords: Transparent conductors; Silver nanowire network; Polycrystalline graphene; Self-heating network; Copercolation transport

1 Introduction

Indium tin oxide (ITO) is a mature technology, but lower-cost, higher-performance alternatives are desired. Transparent conducting electrodes (TCEs) are integral elements in many current and emerging electronic and optoelectronic components, including touchscreens, photovoltaics, displays, thin film transistors (TFTs), and organic light emitting diodes (OLEDs) [1]. Currently, transparent conductive oxides (TCOs) are the most widely used materials for TCEs. While ITO is the most common, TCOs of interest include fluorine-doped tin oxide (FTO) and metal-doped zinc oxides (such as aluminum-doped zinc oxide (AZO)). A relatively large band gap and a very high concentration of free electrons (typically > 10^{20} cm^{-3} in the

Suprem R. Das#: School of Electrical and Computer Engineering, Purdue University, West Lafayette, IN 47907, USA; Birck Nanotechnology Center, Purdue University, West Lafayette, IN 47907, USA; Present address: Iowa State University, Ames, Iowa 50011, USA; Contributed equally to the work
Sajia Sadeque#: School of Electrical and Computer Engineering, Purdue University, West Lafayette, IN 47907, USA; Birck Nanotechnology Center, Purdue University, West Lafayette, IN 47907, USA; Contributed equally to the work
Changwook Jeong, Ruiyi Chen: School of Electrical and Computer Engineering, Purdue University, West Lafayette, IN 47907, USA
***Corresponding Author: Muhammad A. Alam:** School of Electrical and Computer Engineering, Purdue University, West Lafayette, IN 47907, USA; Birck Nanotechnology Center, Purdue University, West Lafayette, IN 47907, USA; Email: alam@purdue.edu
***Corresponding Author: David B. Janes:** School of Electrical and Computer Engineering, Purdue University, West Lafayette, IN 47907, USA; Birck Nanotechnology Center, Purdue University, West Lafayette, IN 47907, USA; Email: janes@purdue.edu
#These authors contributed equally to the work.

conduction band) ensure that TCOs have excellent optical transmission and relatively high electrical conductance, respectively [2, 3]. The technology is mature and mass production of TCO-coated glass (thousands of tons/day) for a broad range of product categories is routine. Unfortunately, TCOs have several limitations: First, there appears to be a fundamental trade-off between carrier concentration and optical absorption, with the dopants or defects required for high carrier concentrations contributing to increased optical absorption [4, 5]. In particular, the n-doping of TCOs arises from intrinsic defects or external doping – these in turn lead to strong absorption in infrared regions of the spectrum, limiting the overall transmission of 85–90%. This may be sufficient for touchscreens, but photovoltaic (PV) technologies could benefit from higher performance alternatives. Second, in addition to conventional Moore's scaling (for high speed/performance computing), "more-than-Moore (MtM) technology" approaches will require flexible and transparent electronics/optoelectronics for applications such as flexible displays and touchscreens [6, 7]. ITO must be sufficiently thick to meet the conductivity requirement, making it difficult to fabricate it as a flexible film. Third, there is limited abundance of elements such as indium; therefore, massive deployment of thin-film PV technology will require materials other than ITO. This has prompted research on materials such as fluorine- or metal-doped oxides as well as nanostructured approaches. These emerging requirements of higher performance, flexibility, earth-abundant supply, and most importantly, the high cost of TCOs have led to extensive research into alternate TCE materials, including nanostructured materials.

The first generation of TCO-alternatives is based on metal nanonets: A number of two-dimensional networks of nanostructured elements have been reported, including metallic nanowire networks consisting of silver nanowires (NWs), metallic carbon nanotubes (m-CNTs), copper nanowires or gold nanowires, and metallic mesh structures [8–12]. In these single-component systems, it has generally been difficult to achieve sheet resistances that are comparable to ITO at a given broadband optical transparency, particularly in the high sheet conductance/high optical transmittance regime.

The second generation of TCO-alternatives is based on copercolating networks: A relatively new third category of TCEs consisting of networks of 1D–1D and 1D–2D nanocomposites (such as silver nanowires and CNTs, silver nanowires and polycrystalline graphene, silver nanowires, and reduced graphene oxide) have demonstrated TCE performance comparable to, or better than, ITO [13–15]. Here we denote this class as "hybrid networks." In such hybrid networks, copercolation between the two components can lead to relatively low sheet resistances at nanowire densities corresponding to high optical transmittance. We denote hybrid networks exploiting copercolation as "co-percolating networks." This review provides an overview of reported hybrid networks, including a comparison of the performance regimes achievable with those of ITO and single-component nanostructured networks. In particular, copercolating networks have been shown to provide superior performance in the high sheet conductance/high optical transmittance regime. The performance is compared to that expected from bulk thin films and analyzed in terms of the copercolation model. In addition, performance characteristics relevant for flexible and transparent applications are discussed, including self-heating and bendability.

The review is arranged as follows: Section 2 provides a systematic comparison of electrical conductance and optical transmission of the three classes of TCEs. Section 3 explains the physical principles that are necessary for the performance of these films and how they are reflected in the performance metrics defined in Section 2. A number of practical and interesting applications have been demonstrated using nanostructured networks and are summarized in Section 4. Section 5 concludes the paper with a discussion regarding the challenges of displacing the traditional, mature, and well-established technology, and frames the progress made in a broader perspective.

2 Performance Comparison of Thin-Film and Nanostructured TCEs

2.1 Selection of Representative Studies

A number of studies have been published for each class of TCEs described in this paper [8–28]. In order to allow qualitative and quantitative comparison among the performance of the three classes of TCEs, representative studies from each class have been selected. In this analysis, representative publications are chosen based on (i) performance (transmittance (T) versus sheet resistance (R_S) relationship), which is representative of high-quality results within the class, (ii) availability of a complete set of data (thin-film thickness (t), nanowire density/thickness, T, R_S or conductivity/resistivity), and (iii) a sufficiently large thickness range, allowing meaningful interpolation or extrapolation of T over a range of ~70% to 90%. In general, a variety of results have been obtained within a given

class, corresponding to different deposition techniques, width and length of nanowires, or postprocessing techniques [16–21]. Most of the studies account for the optical properties of the substrate, typically by correcting for the substrate reflectance and normalizing the measured T values to those measured for the substrate (to compensate for substrate loss).

The classes of TCE and representative studies are the following.

I. Indium Tin Oxide

ITO is a widely used TCO and is chosen as a representative material for TCOs. While materials such as AZO and FTO have shown somewhat lower sheet resistance at a given optical transmittance (compared to ITO) [22, 23], the transmittance versus thickness and sheet resistance versus thickness relationships are expected to be qualitatively similar to those of ITO.

a) Peumans et al. [24], denoted as "ITO theory." The authors simulate T and R_s of ITO thin films based on "optical constants for e-beam deposited ITO acquired using spectroscopic ellipsometry." Since ITO performance varies widely depending on processing details and a widely accepted empirical data set is not available, this theoretical data set is used by many groups to compare the performance of new TCEs. Unfortunately, the paper does not explicitly specify the film thickness.

b) Benoy et al. [25], denoted as "ITO Benoy." This experimental study presents a complete data set (t, R_s, T) for a range of thicknesses, ranging from 80 to 350 nm. In this paper, it was not clear how the authors corrected for substrate reflection and multiple reflections. The data compares well with "ITO theory" for the range of thicknesses reported; however, data regarding the low-resistivity regime is not available.

II. Silver Nanowire and CNT Nanotube Networks

a) *Ruiz et al.* [26], denoted as "AgNW Ruiz." This paper presents a complete set of data with good performance (R_S = 20.2Ω/sq at T = 95%). Data for density, R_S, T are provided along with nanowire dimensions. Several combinations of length and width are reported; the current analysis focused on a specific data set (length ~100 μm and width ~200 nm), which represents the highest performance.

b) *Colman et al.* [27], denoted as "AgNW Colman." This paper also presents a complete set of data, including R_s vs t_{eff}, T vs t_{eff}, T vs R_s. The reported nanowire parameters include length = 6.6 μm and diameter = 84 nm. The effective thickness of the film (t_{eff}) will be defined in Section 2.2.

c) *Lee et al.* [28], denoted as "CNT Lee." This paper presents a relatively complete set of data, including conductivity vs thickness and R_S vs T. The CNT dimensions (diameter, length) are not stated, and thickness data has not been provided for all data points. Data points that are present in both conductivity vs thickness plot and $R_S$vs Tplot are utilized in the current analysis.

III. Hybrid Graphene–Nanowire Copercolating Networks

a) *Chen et al.* [20], denoted as "hybrid, solution cast." Our earlier study presented results on a high-performance hybrid network produced by drop-casting, along with an analysis of R_S extraction from circular transmission-line-model (TLM) test structures. The AgNWs had nominal length/diameter of 40 μm and 100 nm and nominal NW densities were stated.

b) *Peng et al.* [29], denoted as "hybrid graphene/AgNW R2R." This publication presents a high-performance hybrid network, produced by roll-to-roll printing using a AgNW suspension with a length of 20 μm and a diameter of 30 nm and nominal NW densities were stated.

c) *Peng et al.* [30], denoted as "hybrid graphene/nanotrough R2R." In addition to the hybrid AgNW–graphene network, Peng et al. presented results for a hybrid structure consisting of a single layer of graphene and a 2-D network of copper nanotroughs. These samples exhibited very good performance, among the best R_s versus T performance reported to date, particularly in the low R_S/high T regime. In addition, this data set allows direct comparison to hybrid AgNW–graphene networks reported by the same authors. The dimensions and density of the Cu nanotroughs are not given.

2.2 Comparison of Sheet Resistance versus Transmittance Performance

A direct comparison between the reported performances of various TCE is illustrated in Fig. 1, which presents the T versus R_S (log scale) for the various data sets described in the previous section. The graph also includes the modeling result (from [24]), which shows the predicted performance of ITO over a relatively broad range of parameters. For data sets that present points at the same T (R_S), a direct comparison can be made based on the corresponding values of R_S (T). Of the TCE classes considered in this analysis, the hybrid samples, including graphene/AgNW and graphene/Cu nanotrough networks, exhibit the highest overall performance in the high T regime (T ~90% and above). The physical phenomena responsible for the performance in this regime, corresponding to relatively low nanowire/nanotrough densities, will be discussed in

Table 1: Comparison of t_{eff} for representative studies on various classes of TCEs.

TCE type	t_{eff} at 70% T	α_{eff} (cm^{-1})	Density (wires/mm^2)	Density (g/m^2)	Thickness (nm)
ITO Theory	500 nm	N/A			
ITO Benoy	500 nm	3100			80–350
AgNW Ruiz	6900 nm	235		3.5–17.7	
AgNW Colman	210 nm	10,000			64–532
Hybrid, solution cast	28 nm	55,000	$2 \times 10^4 - 4.8 \times 10^4$		
Hybrid graphene/AgNW R2R	3.5 nm	400,000	$2.5 \times 10^4 - 5 \times 10^4$		
Hybrid graphene/nanotrough R2R	8 nm	180,000			
CNT Lee	50 nm	34,000			11 - 87

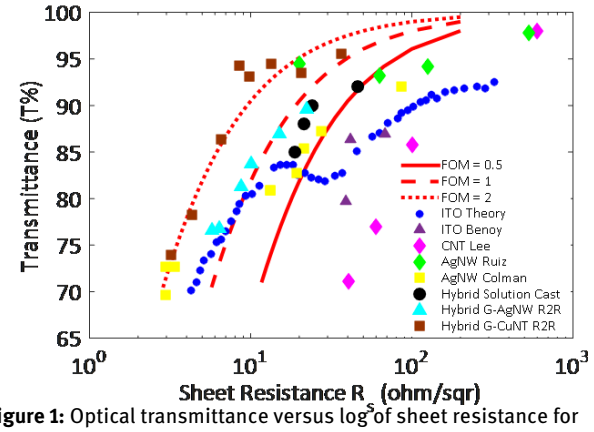

Figure 1: Optical transmittance versus log of sheet resistance for representative studies on various types of transparent conductors. The various studies are summarized in the text.

Section 3. For both ITO and percolating networks, it has proven difficult to achieve comparable G_S values in the $T > 90\%$ regime. The thicknesses dependences of G_S and T in these networks, along with a physical model for the GS versus thickness dependence in a percolating network, will be discussed in later sections.

Note that the overall relationship between R_S and T is qualitatively different between various classes of TCEs. In order to allow comparison with the T vs R_S relationship expected for bulk thin films, and associated with a common definition of a figure of merit (FOM), curves are also shown for three values of the FOM, as stated in the caption. The specific dependences of T and R_S on t will be discussed in a later section, along with a description of the applicability of the FOM.

2.3 "Effective" Thickness of Transparent Conducting Films

The performance of various TCE films may be compared – as we just did in Fig. 1 – without specifying the film thickness. However, a deeper theoretical understanding of the data is possible when the information regarding thickness dependence of transmission and resistance are available. As we will see below, for the new class of TCEs developed over the recent years, the notion is "thickness" is not easy to define; nonetheless, a careful definition allows systematic and meaningful comparison of the data set available.

Typically, in TCEs based on networks of nanostructures, the density of nanowires/nanotubes (D) is presumed to correlate directly with the thickness of a bulk thin film (t). The sheet conductance (G) and optical transmittance (T) are expected to follow, at least qualitatively, the respective bulk thin film dependencies on thickness. In order to allow a more direct comparison between various classes of materials, it is beneficial to define an effective thickness, t_{eff}, for each class of materials. Such a comparison provides a means to quantitatively compare the sheet conductance–transmittance behavior in various networks and to identify regimes in which this behavior deviates from the expected relationships for bulk thin films. For thin film TCOs, including ITO, t_{eff} is t, the actual thickness of the film. For percolating and copercolating networks, we define t_{eff} as the thickness of a uniform thin film of the same material (e.g., Ag in the case of Ag nanowire networks) containing the same number of atoms/cm^2 as the nanostructured network. Note that this definition considers the nanowire–nanotrough–nanotube component, but does not account for the 2-D layer (e.g., graphene). For cases in which the authors have stated film thickness or a comparable quantity, the t_{eff} is determined from the parameters stated in Table 1. The t_{eff} is calculated for the various cases as follows:

a) AgNW Ruiz: Silver density D is given in g/m^2. The t_{eff} is: $1\,\text{cm} \times 1\,\text{cm} \times t_{eff} \times \rho = \frac{D\,(\text{in g/m}^2)}{10000}$.

b) AgNW Colman: t_{eff} is directly given. To show a smooth transition, one data point per t_{eff} has been taken.

c) Hybrid Graphene/AgNW Solution Cast: Silver nanowire density D is given in #of wires/cm^2. The t_{eff} is calculated

from: 1 cm × 1 cm × t_{eff} × ρ = ρ × total volume = ρ × $D\left(\text{in } \frac{\#\text{ of wires}}{\text{cm}^2}\right) \times \pi r^2 l$

d) Hybrid Graphene/AgNW R2R: Here silver nanowire density D is given in #of wires/mm^2. D in #of wires/mm^2 is multiplied by 100 to convert to #of wires/cm^2. The t_{eff} is calculated from: 1 cm × 1 cm × t_{eff} × ρ = ρ × total volume = $\rho \times D\left(\text{in } \frac{\#\text{ of wires}}{\text{cm}^2}\right) \times \pi r^2 l$.

The references 'ITO theory' and 'hybrid graphene/nanotrough R2R' do not report thickness and/or nanowire density, nor do they report dimensions of nanotroughs. In order to obtain t_{eff} for this case, we have assumed that the t_{eff} at T =70% is the same as that calculated for ITO Benoy. Assuming G_s vs t^*_{eff} is linear, the t_{eff} value for a given point can then be directly calculated from the corresponding G_S value. In the case of hybrid graphene/nanotrough R2R, neither dimensions nor density is stated for the nanotroughs. In order to obtain t_{eff} for this case, it is estimated from the reported $G_S$values, assuming the same conductivity value (σ = 400, 000 /ohm-cm) reported for individual nanotroughs. This assumption again implies an assumption that G_s vs t^*_{eff} is linear and yields t_{eff} at T = 70%, which is in the same range as that calculated for hybrid AgNW/graphene samples. Note that the corresponding values for t_{eff} listed in Table 1 (value at T = 70%, shown in bold for these studies) are somewhat arbitrary. However, the relative values between various data points (used for normalized thickness, discussed below) are consistent with the corresponding reported R_S values reported in the respective papers.

2.4 Physical Model for Bulk Material and Adaptation for Nanostructured TCEs

In case of the bulk material, the relation between transmittance (T) and thickness (t) of the material can be written as

$$T = (\exp(-\alpha t))^2 \tag{1}$$

where α is the absorption coefficient. The relation between sheet conductance (G_s) and t can be written as:

$$G_s \equiv R_s^{-1} = \sigma t \tag{2}$$

where σ is the dc conductivity of the material.

For most TCE applications, at least 70% of the light must be transmitted (i.e. $T \geq 0.7$). This regime of interest corresponds to $\alpha t \ll 1$, so that Eq.(1) can be linearized as follows:

$$T \simeq 1 - 2\alpha t \tag{3}$$

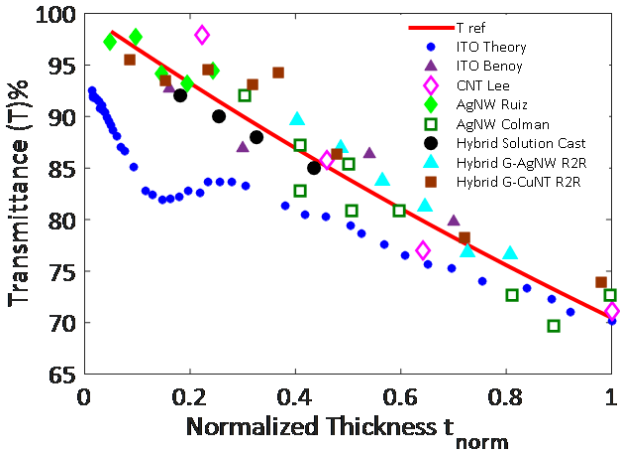

Figure 2: Optical transmittance vs. normalized thickness for representative studies on various types of transparent conductors. A linear relationship (eq. 4b) is also shown for reference. The various studies are summarized in the text.

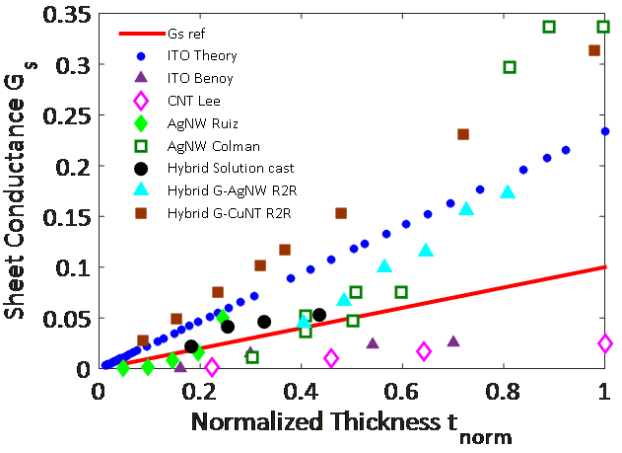

Figure 3: Sheet Conductance versus normalized thickness for representative studies on various types of transparent conductors. A linear relationship (Eq. (4a)) is also shown for comparison. The various studies are summarized in the text.

Assuming that comparable relationships apply for TCEs based on metallic NW/CNT networks and copercolating networks, Equations (2) and (3) can be rewritten in terms of the effective thickness, t_{eff}, so that:

$$G_s \equiv R_s^{-1} = \sigma_{eff} t_{eff} \tag{4a}$$

$$T \simeq 1 - 2\alpha_{eff} t_{eff} \tag{4b}$$

where σ_{eff} and α_{eff} are the corresponding effective electrical conductivity and effective absorption coefficient of the percolating/copercolating film. The "effective" designations refer to spatially average parameters, e.g., effective thickness of a random 2D nanowire network can be

defined in terms of the average thickness over some macroscopic area, while the physical thickness of the layer will vary spatially on a microscopic scale (e.g., on a wire versus a gap in between wires). Strictly speaking, σ_{eff} and α_{eff} are well defined only in the case where the behavior versus thickness follows the relationships in Eqs. (4a) and (4b), respectively. Detailed electromagnetic simulations justify Eq. (4b) for nanonets and metallic nanowire arrays [20, 31], but the justification of Eq. (4a) will be considered more carefully in Section 3. As discussed in this paper, representative reports from percolating networks exhibit sheet conductances that deviate significantly from the relationship in Eq. (4a) over the transmittance range of interest. In this case, it is not possible to define a single value of σ_{eff} that accurately describes the overall relationship. Even for copercolating networks that follow the relationship of Eq. (4a), carrier mobility is not a meaningful quantity, since the carrier density within the network is not known, and conductance is limited by junctions rather than by bulk regions.

In order to represent various classes of materials on a single graph, we define a normalized effective thickness,

$$t_{norm} = \frac{t_{eff}(T)}{t_{eff}(T = 0.7)} \tag{5}$$

i.e., the thickness of the film at 70% transmission is taken as $t_{norm} = 1$. Figs. 2 and 3 present the T versus t_{norm} and G_s versus t_{norm} relationships, respectively, for the representative studies summarized in Table 1. For generating Figs. 2 and 3, data points corresponding to values of T at and above 70% have been considered. Actual experimental T and R_s data has been plotted against t_{norm}. If experimental T and R_S data (at $T = 0.7$) are available, those are used directly to calculate t_{norm}. In case, they are not available, experimental T is fitted with thickness t or t_{eff} with a straight line to infer the thickness t or t_{eff} at 70% transmission.

The value of t_{eff} corresponding to $T = 0.7$ is shown, along with the thickness/density parameter reported in the corresponding paper. The t_{eff} values shown in bold correspond to samples in which density/thickness was not provided (see main text). The α_{eff} values obtained by fitting the reported transmittance versus effective thickness relationships over the range of reported values (effectively using Eq. (4b)) are also shown. In the case of hybrid samples, a pre-factor corresponding to the transmittance of single-layer graphene is employed. The optical transmittance in the "ITO Theory" report does not follow the relationship in Eq. (4b), so a single value for α_{eff} is not suitable to describe the overall relationship.

In case of the three classes of TCEs in our discussion, experimental data shows significant deviations from these equations. For transparent thin film coatings like ITO (e.g. ITO Theory), Gs follows the classical equation, but T deviates at the lower thickness regime (T actually goes down). Moreover, fitting of the T vs $t$data shows a prefactor of 0.9 (instead of 1). Both these effects are likely related to the reflection loss due to multiple scattering from the backside of the material that becomes significant at the low thickness regime. The experimental study considered in this paper (ITO Benoy) contains a relatively small number of data points, so this effect is difficult to observe. However, experimental reports considering a larger number of data points exhibit T vs t relationships that deviate from that presented in Eq. (3).

In case of percolating system like AgNW network (AgNW Ruiz and AgNW Colman), T follows the bulk equation showing a linear gradual decrease with t_{eff} as expected, but G_s does not – rather it shows a sudden decrease in G_s as t_{eff} decreases. The reason behind this is straightforward: as we will see later in Section 3, below the percolation threshold, the network components cannot form a continuous thin film, which is reflected in its poor sheet conductance, G_s. The t_{eff} value at which this occurs (corresponding to the percolation threshold) varies with nanowire dimensions and potentially with deposition technique.

For copercolating network systems (hybrid, solution cast, hybrid graphene/AgNW R2R and hybrid graphene/nanotrough R2R), both T and G_s follow the classical equations, i.e., G_s increases and T decreases linearly with t_{eff}. Fitting of the experimental T vs t_{eff} shows a prefactor of 0.97 (instead of 1). This number represents the transmission of monolayer graphene (97%) when $t = 0$, i.e., when the nanowire network is absent. As will be discussed in detail in a later section, copercolation results in a linear G_s versus T relationship, even at t_{eff} values that would correspond to the "below percolation threshold" regime in single-component nanostructured networks.

2.5 Physical Validity of Typical Figure of Merit

From the discussion above, it can be stated that both thin film (ITO) and percolating networks deviate from expected bulk behavior for film thickness below a critical dimension (due to T effects for ITO and roll-off in G_s for percolating network). With ITO, it may not be possible to attain high T even if the G_s can be increased by doping or thickness. In the case of AgNW or CNT percolating networks, it may not be possible to get high G_s, if one wishes

to retain high T. For photovoltaics applications, however, both T and G_s must be high simultaneously. Copercolating network systems like graphene/metal nanowires and/or graphene/metal nanotrough bridge the gap and ensure high G_s (low R_s) regime, without compromising high T (i.e., at lower t).

A figure of merit (FOM) should allow comparison of the performance of different types of transparent electrodes. The comparison is valid only in the regime where the physical model that has been utilized to construct the FOM accurately describes the behavior of a given TCE. For percolating networks, such comparisons are valid only above the percolation threshold regime. In this study, we employ a modified Jain/Gordon figure of merit [5, 32], namely FOM $\equiv \frac{\sigma_{eff}}{\alpha_{eff}}$. This FOM is consistent with the physical model (e.g., Eqs (4a) and (4b)) discussed in the previous section. It should be noted that neither σ_{eff} nor α_{eff}, in isolation, represent a valid figure of merit for a TCE; one must consider the two together, along with a thickness range over which relationships comparable to Eqs. (4a) and (4b) apply.

Besides comparing the performances of different TCEs, a useful FOM should also allow extrapolation of the behavior of a specific TCE over a broad t_{eff} regime, i.e., to accurately predict how T and R_s change as t_{eff} changes. For copercolating network systems, the thickness dependencies of both T andG_s follow the relationships presented in Eqs. 4a and 4b, so the FOM $\equiv \frac{\sigma_{eff}}{\alpha_{eff}}$ is valid for a broader range of t_{eff}, specifically to the regime corresponding to $T > 90\%$. The presence of a second layer in the hybrid systems (e.g., graphene in the samples reported to date) introduces a prefactor in Eq. 4b, corresponding to the transmittance of the graphene layer. This is generally a perturbation on the expected T vs t_{eff} relationship, modifying the FOM extracted for the material but not qualitatively changing the T vs t_{eff} relationship. On the other hand, in case of percolating systems, within the regime below the percolation threshold, $G_s$falls rapidly as t_{eff} decreases. Therefore, a single $\frac{\sigma_{eff}}{\alpha_{eff}}$ value cannot be valid for both the percolating and sub-percolating regime. Efforts have been made [24] to define a different FOMs for the regime below the percolation threshold. However, the traditional FOMs for TCEs, including the one considered in this study, can only quantify the behavior in the regime above the percolation threshold. While ITO generally follows a linear G_S versus thickness relationship over a large range of thicknesses, the T dependence deviates significantly from the expected relationship (Eq. (4b)), due to reflection/multiple reflection effects. Because of this, ITO does not generally follow the overall relationship implied in the FOM. Therefore, different values of FOM will be extracted in various thickness regimes.

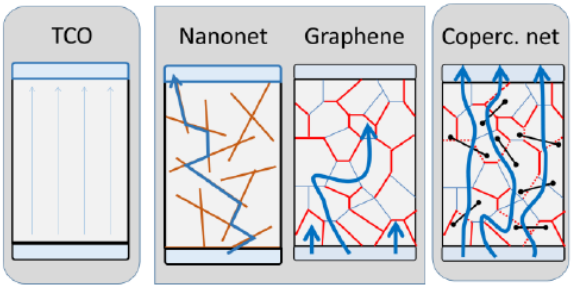

Figure 4: Three generations of TCEs: The TCOs are homogenous ohmic conductors. The Nanonets and graphene both involve conduction through percolating network: the electrons hop from one stick to the next in a nanonet conductor, while they go around the high-resistance grain-boundaries in typical polycrystalline graphene grown in CVD process. The co-percolating network integrates both approaches, and creates a TCO-like conductor with very low percolation threshold. [Part of the image reprinted with permission from reference [52]; Copyright American Chemical Society]

3 Percolation Theory of Transparent Conductors

The discussion above summarizes the progress in TCE development based on phenomenological FOM. The performance differs significantly from one technology to the next. In this section, we will explore the theoretical origin of their transport properties and create a framework to interpret the experimental observations. Schematically the three generations of TCEs are shown in Figure 4.

3.1 TCO Follows Ohm's law

As explained in the previous section, TCOs follow the classic Ohm's law, namely, $G_s = \sigma t$ (see Eq. (2) and Fig. 3). The applicability of Ohm's law simplifies the characterization or optimization of the films. A simple functional form correlates the carrier transport to optical response of these films, as discussed in the previous section [33].

3.2 The Second generation TCO-alternative Films is described by Generalized Percolation Theory

3.2.1 Percolation in AgNW and CNT Nanonet

Nanonets consisting of 2-D networks of various nanostructures, including metallic NWs and semiconduct-

ing/metallic CNTs (s-CNTs/m-CNTs, respectively), have been reported. These TCE films are typically randomly oriented nanowire and/or nanotube networks. This nanonet technology was originally developed for thin-film transistors (TFT), as a high-performance replacement of a-Si [34]. Unlike TFTs, which require semiconducting tubes that can switched on and off by gate voltage, the nanonet TCEs use either purely metallic (e.g., Cu, Ag, Au, Al) or a mixture of metallic and semiconducting elements (e.g., CNTs). The system resembles an ideal stick percolating system [35–40], where carrier travel between any two points of the nanonet by transferring from one wire to the next through the junctions. In 1980s, sophisticated theoretical models were developed to describe the transport through such network. Assuming an ideal system, with zero-resistance junction ($R_J = 0$), the theory predicts the following:

1) Percolation is initiated at a density of $\rho_c = 4.236^2/(\pi L_s^2)$, where L_s is the average length of the nanowire or nanotubes [35–37].

2) For $\rho > \rho_c$, $G = \xi\left(\frac{L_s}{L_c}, \rho_s L_s^2\right) \sim \left(\frac{1}{L_s}\right)\left(\frac{L_s}{L_c}\right)^{m\left(\rho_s L_s^2\right)}$ where the density-dependent exponent m changes from 1.9 (at $\rho \sim \rho_c$) to 1 (at $\rho \gg \rho_c$) [38–40]. Here, ρ_s is the average sheet resistivity and L_c is the critical length.

3) The optical transmittance is correlated to the fractal dimension, D_F. The D_F value increases from 1.57 to 2 with increasing density of tubes. In this sense, a nanonet is neither a 1D stick, nor a 2D film, but a fractional dimensional semiconductor with dimensionality in between [37, 41].

Most nanonets conduct at the percolation threshold (ρ_c), and fractal dimension (D_F) can be correlated to optical transmission. The applicability of the formula for G_s depends on the specific nanonet parameters. The nanotroughs form a continuous film, resembling an ideal network. The other solution-processed nanonets, however, have high R_J values, and the classical expression does not apply directly. For example, the Ag junctions may oxidize over time, s-CNT and m-CNTs can develop a heterojunction, or solution processed films may contain oxidation insensitive wire/wire junctions [42, 43]. The conductance can be suppressed by more than an order magnitude and the exponent may exceed 2 in these networks [44]. Laser annealing or tungsten–halogen lamp exposure can be used to reduce R_J and improve performance [45, 46]. At very high densities, metallic CNTs themselves may percolate without the s-CNTs. The high resistance and variability discussed in Section 2 primarily reflects the influence of the junctions on carrier conduction. Although analytical theory is not available, computational models of stick percolation can consistently interpret the related data [38–40, 47].

3.2.2 Percolation in 2D films such as graphene

A second class of percolating nanonets involves ultrathin transparent films, such as graphene. Graphene deposited by chemical vapor deposition (CVD) is polycrystalline, with average grain-size of a few microns. Each grain is surrounded by high and low resistance grain boundaries [48–50]. The carriers must navigate the maze partitioned by the high-resistance grain boundaries. Therefore, the resistance increases precipitously once the high-resistance boundaries approaches a critical fraction, namely, $\sigma \propto \left(1 - \frac{f_{GB}}{f_{C,GB}}\right)^t \left(\frac{1}{L_c}\right)$, with $t = 1.05 - 1.3$ and $f_{GB} \sim 10 - 12\%$ is the percentage of the total area covered by high-resistance grain boundaries (see Fig. 4). Indeed, conduction in polygraphene seems to precisely be defined by an effective media theory that interpolates between the conduction through the grain and percolation through the grain boundaries. Here ρ_{NW} denotes the nanowire density (number per unit area), R_C denotes the contact resistance between poly-graphene and silver nanowires in Ω-μm, P_{GB} is the fraction of high-resistance grain boundaries, σ is the sheet conductivity and σ_0 is the intra-grain sheet conductivity of poly-graphene. The inset in the left image of Figure 5s shows the Normalized Standard Deviation (NSD) of normalized conductivity vs. percentage high-resistance grain boundaries As shown in Fig. 5, most graphene-based TCEs, therefore, do not meet the minimum requirement of conductivity needed for high-performance applications.

3.2.3 Percolation in 2D films composed of graphene oxides

Solution-processed graphene oxide (GOX) films contain overlapping flakes of GOX though which electrons can percolate from one end of the conductor to the next [51]. The GOX network is analogous to stick percolation, except that the system involves overlapping polygons. Similar to the idealized stick network, significant work has been done regarding idealized percolating network involving polygons, with vanishingly small transfer resistance from one polygon to the next. In practice, the overlap resistance is a key concern, similar to the CNT network, and therefore, despite significant work, the network performance is comparable to CNTs. More work is needed in this direction so that these films to compete with TCO.

3.3 Copercolating Hybrid TCEs Obviates the Percolation Bottlenecks

As shown in Fig. 5, the highest performance TCEs all rely on a two layers system, namely, a metallic nanonet in par-

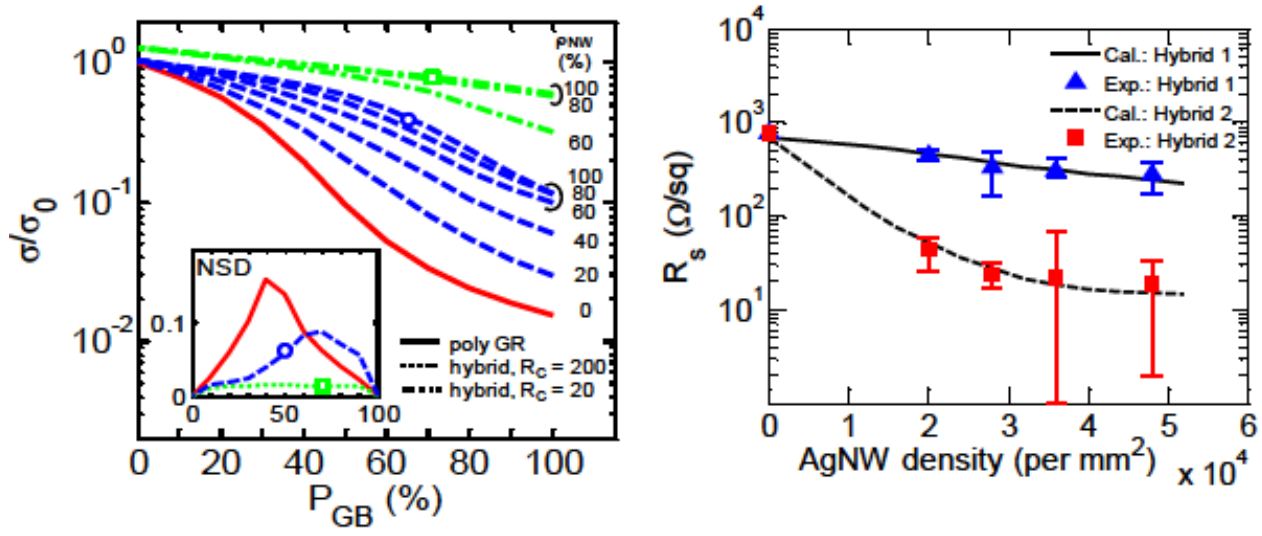

Figure 5: In a co-percolating network, Ag-NWs improve the conduction in graphene. (Left) Theoretical prediction: The conduction in graphene-like 2D polycrystalline films is expected to reduce dramatically with the increase in the fraction of high-resistance grain boundaries. When NWs bridge the GBs, dramatic improvement in resistance is observed. At $\rho_{NW} = 100\%$, the average separation between NWs is 10 µm. (Right) Experimental dependence of sheet resistance on NW density, confirming that the improvement is due to NWs. [Part of the image reprinted with permission from reference [52] and reference [20], respectively; Copyright American Chemical Society & Wiley]

allel with a 2D conductor, such as graphene. As explained in detail in Ref. [26], these hybrid networks should not be viewed as two noninteracting conductors (percolating or otherwise) in parallel – after all, the observed resistances are significantly lower than the parallel combination of the resistances of the two components (measured individually). Instead, graphene grains allow electrons to bypass the highly resistive NW–NW junctions; likewise the NWs bridge the grain boundaries. Together, these elements mutually erase the percolating bottlenecks and reduce the overall percolation threshold. The resistance of the hybrid is lower than the individual films – this is an example of percolation engineering. This is why the FOM of copercolating hybrids behave as if they are classical thin films, except with much higher performance.

Although the nanotrough involved more difficult processing, the network itself has very little tube–tube resistance, and therefore, offers significantly improved performance [30]. Moreover, the use of earth-abundant materials addresses an important criticism of TCO-based technologies.

4 Multifunctional Applications of Copercolating Hybrid TCEs

One of the most important features of the copercolating system (e.g., AgNW–graphene hybrid structure) is its multifunctional use (i.e., electrical, thermal, chemical, mechanical) beyond the original TCE applications. Recently, a number of applications of hybrid AgNW–graphene have been demonstrated in the literature ranging from its use as electrodes in light-emitting diodes to atomically thin barrier layer for protection against high-energy radiation [21, 29, 30, 52–61]. The schematic shown in Figure 6 summarizes the recent progress in the field and Table 2 presents their key physical properties. The applications can be broadly classified as being active vs. passive, as follows.

4.1 Hybrid TCEs as Active Substrate

The electrical transport properties of hybrid films are of primary interest. Theoretically proposed by Jeong et al. [52], percolation doping of nanowires in polycrystalline graphene (involving a "hybrid 1" structure with nanowires deposited over graphene) was observed to provide high transparency and high sheet conductance. Experimental realization and physical insight into the copercolation mechanism were later demonstrated in an inverted structure ("hybrid 2" structure, in which the graphene layer was deposited on top of the nanowire network) [20]. In such a network, the individual transport bottlenecks of nanowire–nanowire junction resistances and graphene grain–boundary resistances were circumvented by each other, leading to stabilized sheet resistance of 13 Ω/□ with $T = 88\%$ at a wavelength of 550 nm. As a result, a number of devices, including the electrochromic device, UV LED, red LED, polymer LED, and organic solar cell, electrodes

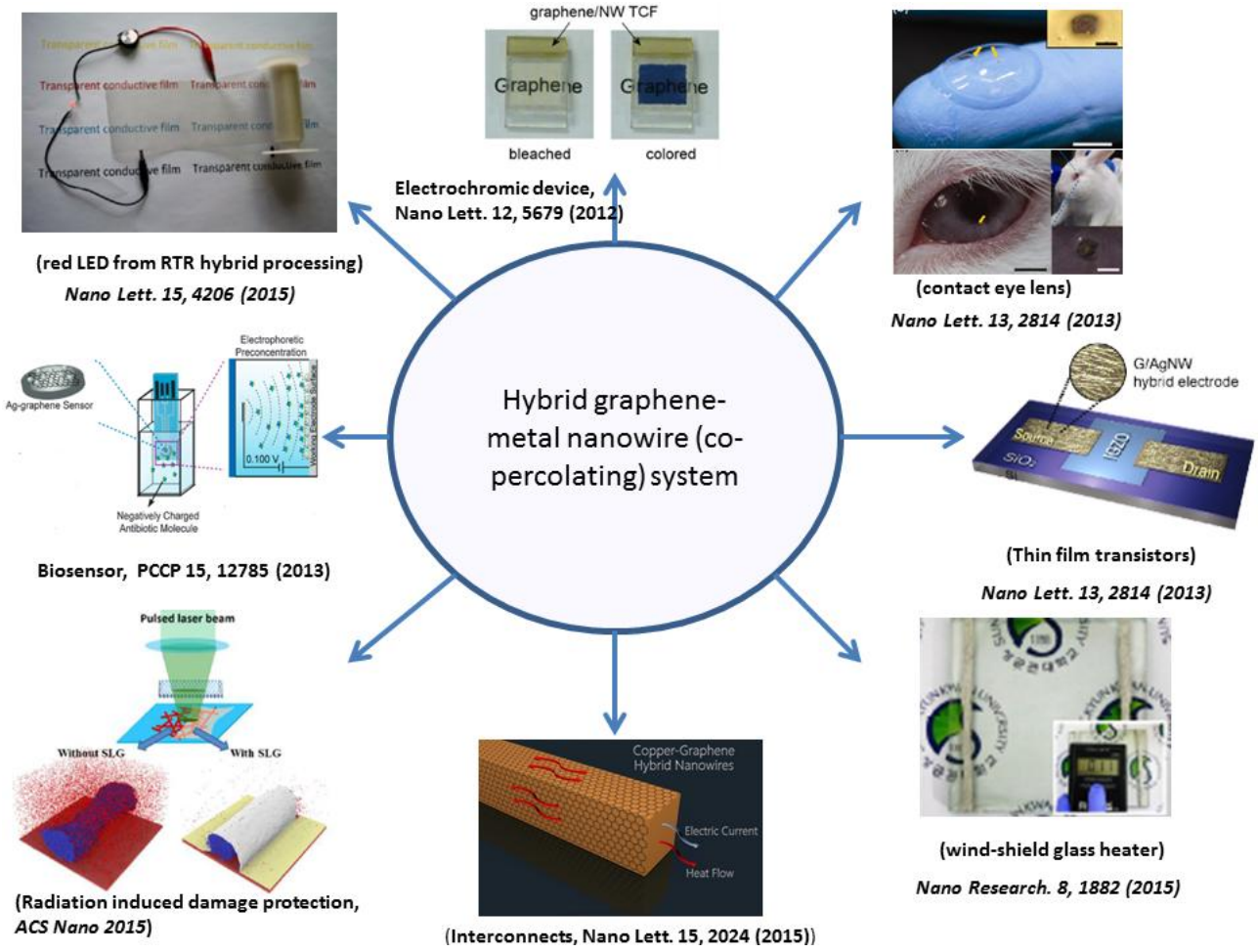

Figure 6: Schematic diagram of multifunctional applications of nanowire-graphene co-percolating system [images/modified images reprinted with permission from references [14, 21, 27, 58, 63, 64, 71] Copyright American Chemical Society, Springer, and Royal Society of Chemistry]

for transistors, and biosensors have been demonstrated as an application of hybrid TCE [20, 21, 53, 55–60] . In addition, hybrid networks have also been used as source and drain electrodes in a transistor structure [21].

Another superior property of hybrid networks is improved heat spreading with respect to that of percolating networks [61–63]. Metal nanowire network-based percolating structures are prone to developing self-heated hotspots that originate primarily from nanowire – nanowire junctions and from conduction through the bodies of the nanowires. In a hybrid network, the graphene layer, intimately coupled to the nanowires, efficiently extracts heat from the hotspots in the underlying nanowire network. The presence of graphene also enables injection of higher current density into the structure, making it robust for applications such as transparent heaters, wind shield glass heater, advanced interconnect structures, etc. [61, 64–66].

The third vital property of hybrid structures is mechanical flexibility, particularly in retaining the electrical performance while undergoing bending cycles. This stability under mechanical bending provides advantages over other classes of TCEs (thin-film ITO and nanonet TCE) for practical applications in bendable and flexible electronics and wearable electronics [67, 68].

4.2 Hybid TCE as a Passive Substrate

There are a number of equally useful passive applications for hybrid networks. In hybrid networks employing graphene as a top layer (e.g., “hybrid 2” described earlier), the graphene provides a barrier layer to atmospheric gasses, and therefore passivates the underlying structure. This property enables applications in a number of other areas, including atmospheric antioxidation and anticorrosion of nanostructures and soft materials, barrier lay-

Table 2: Multifunctional properties of Hybrid nanowire–graphene structure.

Application	Multifunctional property	Mechanism	References
UV LED, polymer LED, solar cell, electrochromic device	Electrical, optical	Copercolation (electronic)	[53, 55–57, 59]
2D atomic layer barrier to light-induced degradation to nanostructures	Thermal, optical	Copercolation (thermal/phonon), thermal conductivity	[73]
Flexible optoelectronic devices	Mechanical, electrical, optical	Strain relaxation, electronic transport	[51, 56, 67]
Transparent flexible heater	Thermal, electrical, optical	Thermal conductivity	[64, 65]
Transparent flexible loud speaker	Acoustic, mechanical, optical		[58]
Flexible transistor S/D contacts	Electrical	Electronic transport	[21]
Flexible biosensors	Electrical, biological	Electronic transport, sensing	[60]
Molecular protection layer/anti-oxidant/anti corrosion	Chemical	Diffusion barrier	[69–72]

ers for biological substances, barrier for copper interconnects, and atomically thin protection layer for nanostructures from radiation-induced damage [69–73]. The atmospheric stability is further discussed in Section 5.2 for various materials of choice for hybrid TCE. Graphene protection could also be used as thinnest possible mask for soft metallic nanostructures to pattern and produce nanophotonic structures [74].

4.3 Scalable manufacturing and possible industrial applications

Both graphene and silver nanowires have previously been shown in roll-to-roll (RTR) manufacturing [75, 76]. Recently, Deng et al. [29] and Chandrashekhar et al. [30] have reported RTR manufacturing of hybrid silver nanowire–graphene films with exceptionally good properties. These efforts have not only provided the prototype laboratory based multifunctional applications of hybrid copercolating TCE, but could also enable mass production of related components.

5 Outlook

The discussion so far has focused on the explaining the improvement in transport properties in TCO-alternative TCEs and a broad range of applications have been demonstrated. It is important to remember that TCO already displays a reasonably good $\sigma - T$ performance; it is a well-tested and mature technology. The new class of TCEs must provide additional benefits to become a disruptive technology. In this regard, we need to consider a number of factors related to availability and reliability of materials that are typically not discussed in detail in many papers.

5.1 Earth Abundance

One of the key concerns for ITO (a TCO) is that indium is expensive and its supply is limited. Unfortunately, some of the TCO alternatives use Ag or Au, which are equally rare (300 ppb and expensive), therefore, would not be suitable for mass deployment. In this case, the use of Cu or Al Nanowire, or carbon nanotubes would be preferred. An important future research direction would involve these earth-abundant resources for fabrication of TCEs. Indeed, among the TCOs, aluminum-doped zinc oxide (AZO) is considerably cheaper. Had it not been a poor moisture barrier, AZO could have replaced ITO in most applications. We will discuss this issue of moisture robustness next.

5.2 Stability in atmospheric conditions

Although Ag-nanowire networks are widely used for demonstration of TCO-alternative technologies, the rapid oxidation of Ag is a key concern [29]. Indeed, the resistance degrades rapidly even after relatively short exposure to environment and long-term stability is also poor. Indeed, the

corrosion resistance of Cu–NT nanonets is not significantly better [29]. Nanonets based on other materials (e.g., Au, Pd) are expected to be more stable, however, stability data are often not available. In this regard, CNT-nanonet performs better than metallic nanonets [28]. In general, copercolating networks are far more stable, even those with Ag and Cu nanowires [20, 29]. Here, the graphene works as a barrier to moisture to prevent oxidation and corrosion. Experiments show stable resistance even after years of exposure to moisture [20, 61].

5.3 Stability against Self-heating

In PV applications, TCEs must carry significant current and self-heating of the film is inevitable. Self-heating in nanonet TCEs have been characterized carefully and in detail. It has been demonstrated that percolation plays an important role in heat conduction in these networks [63], the thermal bottlenecks are reflected in the formation of hotspots and the heating in these hotspots scales superlinearly with current [61], and most importantly, hotspots may eventually seed the fracture of the film [77]. Obviously, self-heating will accelerate oxidation and corrosion of the films.

Copercolating networks reduce self-heating dramatically, as they provide a very efficient thermal-resistant pathway to dissipate heat [61]. Indeed, the heat removal is so effective that it can dissipate heating associated with laser pulses [73]. As a result, the third generation TCO alternatives are expected to be much more reliable. It would be important to demonstrate this feature experimentally.

5.4 Reliability against repeated flexing

A substrate of thickness $2h$ can bend with a radius of curvature R, so long the strain, $\epsilon = h/R$, does not exceed the yield strain ($\epsilon_c \sim 0.1\%$) of the film. As a result, simple and/or composite film must be sufficiently thin (~100 um) so that it is flexible [78]. Therefore, one can create flexible PV by replacing the thick glass substrate (few mm) by thinner substrate involving steel, aluminum, or plastic (25–100 um), and by changing the absorber from thick silicon (~few hundreds of micron) to thinner CdTe or CIGS films (~few hundreds of nanometres). Since ITO is sufficiently thin (~100 nm), therefore, unless the radius of curvature is extremely small (e.g. < 20 mm, Ref. [20, 29]), TCO-based flexible solar cells are viable.

The TCO alternatives are typically thinner. Therefore, flexibility should and does improve [Hybrid R2R]. However, nanonets involve tube–tube junction that may detach under repeated flexing – with a corresponding degradation in resistance [20, 29]. For copercolating network, the wrapping by graphene sheet provides mechanical support and prevents detachment even at stress levels of 100 kPa [20]. Therefore, copercolating networks offers performance comparable or better than ITO films. Another important concern for new generation of TCEs is that the films are bonded to the underlying substrate by van der Walls forces, therefore, the surface may scratch or delaminate under repeated bending. Here, the key idea is that the intralayer bonding strength γ is sufficiently strong so that the strain (ϵ) developed due to flexing remains below the critical strain ϵ_c of the bilayer, i.e.,

$$\epsilon < \epsilon_c = \epsilon_P + \sqrt{(2\gamma/2L)}.$$

Here, ϵ_P is the Poisson buckling ratio and L is the linear dimension of the substrate. Ref. [27] shows that AgNW fails scotch-tape tests, but CNT offers performance. Therefore, interface preparation would be essential for the success of the technology. Overall, it is important to define quantitative metrics for technology comparison.

5.5 Challenges for Alternative TCE Materials

While nanostructured approaches, particularly the copercolating networks, can provide impressive TCE performance as well as the other characteristics described in this the preceding subsections, there are a number of questions that must be addressed before this class of materials are suitable for widespread use. Most of the reported studies to date have focused on overall sheet resistance versus transmittance relationships. Studies on the microscopic conduction physics have shown spatial inhomogeneity on size scales ranging from the nanoscale to hundreds of microns, as well as local behavior that is different from macroscopic behavior (e.g., terminal characteristics [61]). A complete understanding of the conduction physics, as well as understanding of contact properties such as effective work function or barrier heights to various device layers, will be essential in understanding the overall impact on the properties of devices employing these materials. In contrast to studies employing large-size (hundreds of microns), lithographically defined metallic lead frames, the nanostructured nature of these films would be consistent with distributed conduction pathways, e.g. for efficient collection of photogenerated carriers in a photovoltaic device. However, detailed studies of these carrier collection pathways are not yet available. Large-area/high-volume applications will also require alternative deposition methods, such as the roll-to-roll approaches considered in some reported studies [29, 30].

Finally, one might ask whether there are fundamental limits to the TCE performance that can be achieved with these materials. A relatively small portion of the potential parameter space has been explored, and it is likely that new material combinations will yield improvements in the transmittance versus sheet resistance relationship, as well as other performance metrics of relevance to specific applications. Reports to date have considered various diameter–length parameters, and noncylindrical structures such as nanotroughs. A clear optimum solution has not been found at this point, but an advanced understanding of the conduction mechanisms and spatial distribution of conductive pathways/resistive bottlenecks will allow such optima to be modeled. The randomly distributed networks explored to date are realizable with techniques such as printing, but result in a significant fraction of nanowires or nanotubes that are not contributing strongly to the conduction process. Specific alignment strategies can yield improvements in the overall conductance at a given nanowire density, albeit at the expense of more complex processing.

6 Conclusions

In this paper, we have compared several different technologies alternative to TCO. While the T vs R_S relationship allows direct performance comparison between two data points, a more physical-based understanding of the potential performance requires consideration of the dependences of T and R_S on t_{eff}. The physical origin of these effects can be explained by invoking generalized percolation and copercolation theories. We have discussed the importance of defining regimes over which a FOM is applicable, in order to allow a meaningful comparison between various studies. The TCO alternatives have already been demonstrated in a number of applications, suggesting that films are suitable for a broad class of application. The requirements of earth abundance and long-term reliability can steer efforts to design and optimize new generations of TCE to replace TCOs.

Acknowledgement: This work was supported in part by the National Science Foundation (NSF) [Award No. ECCS-1408346].

References

[1] Lewis B. G., Paine D. C. Applications and processing of transparent conducting oxides. MRS. Bulletin. 2000; 25 (8): 22–27.

[2] Kilic C., Zunger A. Origins of coexistence of conductivity and transparency. Phys. Rev. Lett. 2002; 88 (9): 095501.

[3] Liu H., Avrutin V., Izyumskaya N., Ozgur U., Morkoc H. Transparent conducting oxides for electrode applications in light emitting and absorbing devices. Superlattices and Microstructures 2010; 48 (5): 458–484.

[4] Chopra K. L., Major S., Pandya D. K. Transparent conductors – A status review. Thin Solid Films 1983; 102 (1): 1–46.

[5] Gordon R.G. Criteria for choosing transparent conductors. MRS. Bulletin 2000; 25 (8): 52–57.

[6] De Volder M. F. L., Tawfick S. H., Baughman R. H., Hart A. J. Carbon Nanotubes: Present and Future commercial applications. Science 2013; 339: 535–539.

[7] Roy K., Byunghoo J., Than A. R. Integrated systems in the More-than-Moore era: designing low-cost energy-efficient systems using heterogeneous components. 23rd IEEE Int. Conf. on VLSI Design Bangalore 2010; pp. 464–469; DOI 10.1109/VLSI.Design.2010.84

[8] Hu L., Kim H. S., Lee J. Y., Peumans P., Cui Y. Scalable coating and properties of transparent, flexible, silver nanowire electrodes. ACS Nano 2010; 4: 2955–2963.

[9] Wu Z., Chen Z., Du X., Logan J. M., Sippel J., Nicolou M., Kamaras K., Reynolds J. R., Tanner D. B., Hebard A. F., Rinzler A. G. Transparent, conductive carbon nanotube films. Science 2004; 305: 1273–1276.

[10] Zhang D., Wang R., Wen M., Weng D., Cui X., Sun J., Li H., Lu Y. Synthesis of ultralong copper nanowires for high-performance transparent electrodes. J. Am. Chem. Soc. 2012; 134: 14283–14286.

[11] Lyons P. E., De S., Elias J., Schamel M., Philippe L., Bellew A. T., Boland J. J., Coleman J. N. High-performance transparent conductors from networks of gold nanowires. J. Phys. Chem. Lett. 2011; 2: 3058–3062.

[12] Van de Groep J., Spinelli P., Polman A. Transparent conducting silver nanowire networks. Nano Lett. 2012; 12: 3138–3144.

[13] Tokuno T., Nogi M., Jiu J., Suganuma K. Hybrid transparent electrodes of silver nanowires and carbon nanotubes: a low temperature solution process. Nanoscale Research Letters 2012; 7: 281.

[14] Kholmanov I. N., Magnuson C. W., Aliev A. E., Li H., Zhang B., Suk J. W., Zhang L. L., Peng E., Mousavi S. H., Khanikaev A. B., Piner R., Shvets G., Ruoff R. S. Improved electrical conductivity of graphene films integrated with metal nanowires. Nano Lett. 2012; 12: 5679–5683.

[15] Ahn Y., Jeong Y., Lee Y. Improved Thermal oxidation stability of solution-processable silver nanowire transparent electrode by reduced graphene oxide. ACS Appl. Mater. Interfaces 2012; 4: 6410–6414 (2012).

[16] Ishibashi S., Higuchi Y., Ota Y., Nakamura K. Low resistivity indium-tin oxide transparent conductive films. II. Effect of sputtering voltage on electrical property of films. J. Vac. Sci. Technol. A 1990; 8: 1403–1406.

[17] Tang W., Cameron D. C. Aluminum-doped zinc oxide transparent conductors deposited by sol-gel process. Thin Solid Films 1994; 238: 83–87.

[18] Madaria A. R., Kumar A., Ishikawa F. N., Zhou C. Uniform, highly conductive, and patterned transparent films of a percolating silver nanowire network on rigid and flexible substrates using dry transfer technique. Nano Res. 2010; 3: 564–573.

[19] Scardaci V., Coull R., Lyons P. E., Rickard D., Coleman J. N. Spray deposition of highly transparent, low-resistance networks of silver nanowires over large areas. Small 2011; 7: 2621–2628.
[20] Chen R., Das S. R., Jeong C., Khan M. R., Janes D. B., Alam M. A. Co-percolating graphene-wrapped silver nanowire network for high performance, highly stable, transparent conducting electrodes. Adv. Funct. Mater. 2013; 23 (41): 5150–5158.
[21] Lee M.–S., Lee K., Kim S.–Y., Lee H., Park J., Choi K.–H., Kim H.–K., Kim D.–G., Lee D.–Y., Nam S., Park J.–U. High-Performance, Transparent, and Stretchable Electrodes Using Graphene-Metal Nanowire Hybrid Structures. Nano Lett. 2013; 13(6): 2814–2821.
[22] Hagendorfer H. et al., Highly transparent and conductive ZnO:Al thin films from a low temperature aqueous solution approach. Adv. Mater. 2014; 26: 632–636
[23] Kim H., Auyeung R. C. Y., Pique A. Transparent conducting F-doped SnO_2 thin films grown by pulsed laser deposition. Thin Solid Films 2008; 516: 5052–5056.
[24] Lee J.–Y., Connor S. T., Cui Y., Peumans P. Solution-processed metal nanowire mesh transparent electrodes. Nano letters. 2008; 8: 689–692.
[25] Benoy M. D., Mohammed E. M., Suresh Babu M., Binu P. J., Pradeep B. Thickness dependence of the properties of indium tin oxide (ITO) FILMS prepared by activated reactive evaporation. Brazilian Journal of Physics 2009; 39: 629.
[26] Andres L. J., Menendez M. F., Gomez D., Martinez A. L., Bristow N., Kettle J. P., Menendez A., Ruiz B. Rapid synthesis of ultralong silver nanowires for tailor-made transparent conductive electrodes: proof of concept in organic solar cells. Nanotechnology 2015; 26 (26): 265201.
[27] De S., Higgins T. M., Lyons P. E., Doherty E. M., Nirmalraj P. N., Blau W. J., Boland J. J., Coleman J. N. Silver nanowire networks as flexible, transparent, conducting films: extremely high DC to optical conductivity ratios. ACS Nano 2009; 3 (7): 1767–1774.
[28] Geng H.–Z., Kim K. K., So K. P., Lee Y. S., Chang Y., Lee Y. H. Effect of acid treatment on carbon nanotube-based flexible transparent conducting films. J. Am. Chem. Soc. 2007; 129 (25): 7758–7759.
[29] Deng B., Hsu P.–C., Chen G., Chandrashekhar B. N., Lioa L., Ayitimuda Z., Wu J., Guo Y., Lin L., Zhou Y., Aisijiang M., Xie Q., Cui Y., Liu Z., Peng H. Roll-to-roll encapsulation of metal nanowires between graphene and plastic substrate for high-performance flexible transparent electrodes. Nano Lett. 2015; 15 (6): 4206–4213.
[30] Chandrashekar B. N., Deng B., Smitha A. S., Chen Y., Tan C., Zhang H., Peng H. Liu Z. Roll-to-roll green transfer of CVD graphene onto plastic for a transparent and flexible triboelectric nanogenerator. Adv. Mater. 2015; 27 (35): 5210–5216.
[31] Fang J., Das S. R., Prokopeva L. J., Shalaev V. M., Janes D. B., Kildishev A. V. Time-domain modeling of silver nanowires-graphene transparent conducting electrodes. Proc. SPIE 8806, Metamaterials: Fundamentals and Applications VI, 880601 (September 11, 2013); DOI: 10.1117/12.2026871.
[32] Jain V. K., Kulshreshtha A. P. Indium-tin-oxide transparent conducting coatings on silicon solar cells and their "figure of merit". Sol. Energy Mater. Sol. Cells 1981; 4 (2): 151–158.
[33] Schroder D. K. Semiconductor material and device characterization, 3rd Edition, ISBN: 978-0-471-73906-7, June 2015, Wiley-IEEE Press.
[34] Cao Q., Kim H.–S., Pimparkar N., Kulkarni J. P., Wang C., Shim M., Roy K., Alam M. A., Rogers J. A. Medium-scale carbon nanotube thin-film integrated circuits on flexible plastic substrates. Nature 2008; 454 (7203): 495–500.
[35] Balberg I., Binenbaum N. Computer study of the percolation threshold in a two-dimensional anisotropic system of conducting sticks. Physical Review B 1983; 28 (7): 3799.
[36] Li J., Zhang S.–L. Finite-size scaling in stick percolation. Physical Review E 2009; 80 (4): 040104.
[37] Stauffer D., Aharony A. Introduction to Percolation Theory, Revised 2nd Ed. Taylor and Francise, 1994.
[38] Pimparkar N., Cao Q., Kumar S., Murthy J. Y., Rogers J., Alam M. A. Current–Voltage Characteristics of Long-Channel Nanobundle Thin-Film Transistors: A "Bottom-Up" Perspective. Electron Device Letters, IEEE 2007; 28 (2): 157–160.
[39] Pimparkar N., Kocabas C., Kang S. J., Rogers J., Alam M. A. Limits of performance gain of aligned CNT over randomized network: Theoretical predictions and experimental validation. Electron Device Letters, IEEE 2007; 28 (7): 593–595.
[40] Kumar S., Murthy J. Y., Alam M. A. Percolating conduction in finite nanotube networks. Physical review letters 2005; 95 (6): 066802.
[41] Nair P. R., Alam M. A. Dimensionally frustrated diffusion towards fractal adsorbers. Physical review letters 2007; 99 (25): 256101.
[42] Go J., Sysoev V. V., Kolmakov A., Pimparkar N., Alam M. A. A novel model for (percolating) nanonet chemical sensors for microarray-based E-nose applications, IEEE International Electron Devices Meeting (IEDM 2009). 2009.
[43] Ternon C., Serre P., Lebrun J. M., Brouzet V., Legallais M., David S., Luciani T., Pascal C., Baron T., Missiaen, J. M. Low Temperature Processing to Form Oxidation Insensitive Electrical Contact at Silicon Nanowire/Nanowire Junctions. Advanced Electronic Materials 2015; 1 (10): DOI: 10.1002/aelm.201500172
[44] Pimparkar N., Alam M. A. A "bottom-up" redefinition for mobility and the effect of poor tube–tube contact on the performance of CNT nanonet thin-film transistors. Electron Device Letters, IEEE 2008; 29 (9): 1037–1039.
[45] Spechler J. A., Arnold C. B. Direct-write pulsed laser processed silver nanowire networks for transparent conducting electrodes. Appl. Phys. A 2012; DOI: 10.1007/s00339-012-6958-7
[46] Garnett E. C., Cai W., Cha J. J., Mahmood F., Connor S. T., Christoforo M. G., Cui Y., McGehee M. D., Brongersma M. L. Self-limited plasmonic welding of silver nanowire junctions. Nature Materials 2012; 11:241–249.
[47] Gruner G. Carbon nanotube films for transparent and plastic electronics. J. Mater. Chem. 2006; 16 (35): 3533–3539.
[48] Yazyev O. V., Louie S. G. Electronic transport in polycrystalline graphene. Nature Materials 2010; 9: 806–809.
[49] Yu Q. et al. Control and characterization of individual grains and grain boundaries in graphene grown by chemical vapor deposition. Nature Materials 2011; 10:443–449.
[50] Chen R., Das S. R., Jeong C., Janes D. B., Alam M. A. Exclusive electrical determination of high-resistance grain-boundaries in poly-graphene. IEEE Proc. 70th Annual Device research conference (DRC) 2012: 57–58; DOI: 10.1109/DRC.2012.6257034
[51] Eda G., Fanchini G., Chhowalla M. Large Area Ultrathin films of reduced graphene oxide as a transparent and flexible electrode material. Nature Nanotechnology 2008; 3: 270–274.
[52] Jeong C., Nair P., Khan M., Lundstrom M., Alam M. A. Prospects for Nanowire-Doped Polycrystalline Graphene Films for Ultratransparent, Highly Conductive Electrodes. Nano Lett. 2011; 11:

5020–5025
[53] Kholmanov I. N., Domingues S. H., Chou H., Wang X., Tan C., Kim J.–Y., Li H., Piner R., Zarbin A. J. G., Ruoff R. S. Reduced Graphene Oxide/Copper Nanowire Hybrid Films as High-Performance Transparent Electrodes. ACS Nano 2013; 7: 1811–1816.
[54] Chen J., Bi H., Sun S., Tang Y., Zhao W., Lin T., Wan D., Huang F., Zhou X., Xie X., Jiang M. Highly Conductive and Flexible Paper of 1D Silver-Nanowire-Doped Graphene. ACS Appl. Mater. Interfaces 2013; 5: 1408–1413.
[55] Liang J., Li L., Tong K., Ren Z., Hu W., Niu X., Chen Y. Pei Q. Silver Nanowire Percolation Network Soldered with Graphene Oxide at Room Temperature and Its Application for Fully Stretchable Polymer Light-Emitting Diodes. ACS Nano 2014; 8: 1590–1600.
[56] Lee D., Lee H., Ahn Y., Jeong Y., Lee D.–Y., Lee Y. Highly stable and flexible silver nanowire–graphene hybrid transparent conducting electrodes for emerging optoelectronic devices. Nanoscale 2013; 5: 7750–7755.
[57] Liu Y., Chang Q., Huang L. Transparent, flexible conducting graphene hybrid films with a subpercolating network of silver nanowires. J. Mater. Chem. C 2013; 1: 2970–2974.
[58] Xu S., Man B., Jiang S., Liu M., Yang C., Chen C., Zhang C. Graphene–silver nanowire hybrid films as electrodes for transparent and flexible loudspeakers. CrystEngComm, 2014; 16: 3532–3539.
[59] Seo T. H., Kim B. K., Shin G., Lee C., Kim M. J., Kim H., Suh E. –K. Graphene-silver nanowire hybrid structure as a transparent and current spreading electrode in ultraviolet light emitting diodes. Appl. Phys. Lett. 2013; 103: 051105.
[60] Yin P. T., Kim T. –H., Choi J. –W., Lee K. –B. Prospects for graphene–nanoparticle-based hybrid sensors. Phys.Chem. Chem. Phys.2013; 15: 12785–12799.
[61] Maize K., Das S. R., Sadeque S., Mohammed A. M. S., Shakouri A., Janes D. B., Alam M. A. Super-Joule heating in graphene and silver nanowire network. Appl. Phys. Lett. 2015; 106: 143104.
[62] Kumar S., Pimparkar N., Murthy J. Y., Alam M. A. Self-consistent electrothermal analysis of nanotube network transistors. Journal of Applied Physics 2011; 109 (1): 014315.
[63] Kumar S., Alam M. A., Murthy J. Y. Effect of percolation on thermal transport in nanotube composites. Applied Physics Letters 2007; 90 (10): 104105.
[64] Celle C., Mayousse C., Moreau E., Basti H., Carella A., Simonato J.–P. Highly flexible transparent film heaters based on random networks of silver nanowires. Nano Res. 2012; 5 (6): 427–433.
[65] Lee S. M., Lee J. H., Bak S., Lee K., Li Y., Lee H. Hybrid windshield-glass heater for commercial vehicles fabricated via enhanced electrostatic interactions among a substrate, silver nanowires, and an over-coating layer. Nano Res. 2015; 8 (6): 1882–1892.
[66] Mehta R., Chugh S., Chen Z. Enhanced electrical and thermal conduction in graphene-encapsulated copper nanowires. Nano Lett. 2015; 15 (3): 2024–2030.
[67] Li Y., Cui P., Wang L., Lee H., Lee K., Lee H. Highly bendable, conductive, and transparent film by an enhanced adhesion of silver nanowires. ACS Appl. Mater. Interfaces 2013; 5: 9155–9160.
[68] Neves A. I. S., Bointon T. H., Melo L. V., Russo S., de Schrijiver I., Craciun M. F., Alves H. Transparent conductive graphene textile fibers. Scientific Reports 2015; 5: Article number: 9866; DOI: 10.1038/srep09866
[69] Chen S. et al. Oxidation resistance of graphene-coated Cu and Cu/Ni alloy. ACS Nano 2011; 5 (2): 1321–1327.
[70] Bohm S. Graphene against corrosion. Nature Nanotechnology 2014; 9: 741–742.
[71] Zhang W., Lee S., McNear K. L., Chung T. F., Lee S., Lee K., Crist S. A., Ratliff T. L., Zhong Z., Chen Y. P., Yang C. Use of graphene as protection film in biological environments. Scientific Reports 2014; 4, Article number: 4097; DOI: 10.1038/srep04097
[72] Goli P., Ning H., Li X., Lu C. Y., Novoselov K. S., Baladin A. A. Thermal properties of graphene-copper-graphene heterogeneous films. Nano Lett. 2014; 14 (3): 1497–1503.
[73] Das S. R., Nian Q., Saei M., Jin S., Back D., Kumar P., Janes D. B., Alam M. A., Cheng G. J. Single-layer graphene as a barrier layer for intense UV laser-induced damages for silver nanowire network. ACS Nano 2015; DOI: 10.1021/acsnano.5b04628
[74] Zhu B., Ren G., Gao Y., Yang Y., Lian Y., Jian S. Graphene-coated tapered nanowire infrared probe: a comparison with metal coated probes. Optics Express 2014; 22 (20): 24096–24103.
[75] Bae S. et al. Roll-to-roll production of 30-inch graphene films for transparent electrodes. Nature Nanotechnology 2010; 5: 574–578.

[76] Angmo D., Andersen T. R., Bentzen J. J., Helgesen M., Sondergaard R. R., Jorgensen M., Carle J. E., Bundgaard E., Krebs F. C. Roll-to-roll printed silver nanowire semitransparent electrodes for fully ambient solution-processed tandem polymer solar cells. Adv. Funct. Mater. 2015; 25 (28): 4539–4547.

[77] Gupta M. P., Behnam A., Lian F., Estrada D., Pop E., Kumar S. High field breakdown characteristics of carbon nanotube thin film transistors. Nanotechnology 2013; 24: 405204.

[78] Gordon J. Structures: Or Why Things Don't Fall Down (2003). Da Capo Press, 2nd Edition